High pressure phase transition in metallic LaB_6: Raman and X-ray diffraction studies

Pallavi Teredesai[a], D.V.S. Muthu[a], N. Chandrabhas[b], S. Meenakshi[c], V. Vijayakumar[c], P. Modak[c], R.S. Rao[c], B.K. Godwal[c], S.K. Sikka[c], A.K. Sood[a,b,*]

[a]*Department of Physics, Indian Institute of Science, Bangalore 560 012, India*
[b]*Jawaharlal Nehru Center for Advanced Scientific Research, Jakkur Campus, Jakkur P.O., Bangalore 560 064, India*
[c]*High Pressure Physics Division, Bhabha Atomic Research Center, Mumbai 400085, India*

Abstract

High pressure Raman and angle dispersive X-ray diffraction (ADXRD) measurements on the metallic hexaboride LaB_6 have been carried out upto the pressures of about 20 GPa. The subtle phase transition around 10 GPa indicated in Raman measurements is confirmed by ADXRD experiments to be a structural change from cubic to orthorhombic phase. Ab-initio electronic band structure calculations using full potential linear augmented plane wave method carried out as a function of pressure show that this transition is driven by the interception of Fermi level by electronic band minimum around the transition pressure.

Keywords: A. LaB_6; C. Raman scattering; C. X-ray diffraction; E. High pressure

1. Introduction

Hexaborides (MB_6) can be monovalent metals or semiconductors [1] depending on whether the metal ion M is trivalent or divalent, respectively, because the B_6 molecule in them needs two electrons from the metal to stabilize the divalent B_6 state. LaB_6, a monovalent and non-magnetic metal, is of great technological importance as thermionic cathodes in electronic devices with high performance characteristics [2]. In the intermediate valence compounds CeB_6 and SmB_6, the elastic constant C_{12} is negative while in LaB_6 it has a very small positive value [3–5]. The breakdown of Cauchy relation (small value of C_{12} compared to the larger C_{44}) in LaB_6 is an indication of presence of volume-dependent long range forces. Such long range forces are speculated to be arising due to the occupied part of the conduction band formed by the anti-bonding orbitals of the B_6 molecules and the 5d e_g-orbitals of La atoms [6]. The fact that volume dependence can lead to violation of Cauchy relation and the small value of C_{12}, is evident from the behavior of C_{12} and C_{44} of mixed valence $Sm_{1-x}Y_xS$ with variable metal size and the divalent YbB_6 [5]. Application of pressure will result in an energy shift of the anti-bonding B_6 orbitals leading to a rise in the conduction band causing further lowering of C_{12} to induce structural changes under pressure. However, the pressure variation of electrical resistance and thermoelectric power of LaB_6 up to 10 GPa show a monotonic decrease [7] while that of divalent YbB_6 and EuB_6 suggest [8] evidence of mixed valence state at pressures above 10 GPa. The present work aims to investigate the high pressure behavior of LaB_6 experimentally using Raman and X-ray diffraction measurements. Also the first principles electronic band structure

method of full potential linearized augmented plane wave (FPLAPW) type is employed to find the cause of the structural evolution of LaB_6 under pressure.

2. Experiment

High pressure Raman measurements were carried out on single crystals of LaB_6 in a Mao-Bell type diamond anvil cell (DAC) with the excitation line 5145 Å of an argon ion laser and the spectra were recorded at room temperature using Spex Ramalog spectrometer with cooled photomultiplier tube as well as DILOR XY spectrometer with CCD detection [9]. To understand the results of Raman experiments, angle dispersive X-ray diffraction (ADXRD) measurements up to 20 GPa were carried out on powdered LaB_6. For both Raman and X-ray diffraction measurements, the pressure transmitting medium used was methanol + ethanol mixture in 4:1 proportion and ruby fluorescence was used for in-situ pressure calibration. The ADXRD measurements were carried out using a setup [10] which employs graphite monochromatised Mo Kα radiation from a Rigaku rotating anode generator operating at 50 KeV × 40 mA and an image plate (IP) flat area detector (Molecular Dynamics). The stored two dimensional X-ray image of the diffraction rings was scanned at a resolution of $176 \times 176\ \mu m^2$. The gasket material used for the measurements is hardened stainless steel. The sample to IP distance was calibrated by collecting the diffraction pattern of Pd foil loaded in the DAC at ambient condition. The two dimensional image was collapsed to the one dimensional diffraction pattern by radially integrating the stored image using the calibrated sample to IP distance. A correction for the small tilt of the image plate to the beam direction was also employed. Typical exposure time was 4–5 h.

3. Results and discussion

3.1. Raman scattering

The divalent and trivalent metal hexaborides (MB_6) crystallize in the cubic CsCl structure (space group O_h) with one molecule per unit cell [1]. Each B_6 octahedron is centered at the corner of the simple cubic cell with boron atoms located at the cube edges. Group theory yields the wavevector $k = 0$ normal modes as $A_{1g}(R) + E_g(R) + T_{1g} + T_{2g}(R) + 2T_{1u} + T_{2u}$ where R denotes Raman active mode. Fig. 1 shows the unpolarized Raman spectra of LaB_6 recorded at ambient pressure. The three expected main peaks were observed at 677 (T_{2g}), 1116 (E_g) and 1251 (A_{1g}) cm^{-1}, in agreement with earlier reports [1,11–13]. The inset in Fig. 1 shows the eigenvectors of these three intramolecular vibrations of the B_6 molecule [1]. Here, A_{1g} and E_g are B–B bond stretching modes and T_{2g} mode is a B–B–B valence angle bending mode of boron lattice. Raman band associated with T_{2g} mode shows a clear shoulder on the high frequency side and is attributed [11–13] to the most abundant isotopes of B, namely B^{11}/B^{10}. Accordingly, the observed lineshape is least square fitted to a sum of two Lorentzians with an area ratio of A_1/A_2 = 2.1:1 to take into account isotopic ^{11}B:^{10}B abundance. The two peaks are at 677 and 690 cm^{-1}. As is clear in Fig. 1, the E_g mode is a doublet with mode frequencies at 1116 and 1135 cm^{-1}. There is also a weak peak at 1159 cm^{-1}. In Fig. 1, data are shown with open circles and solid lines correspond to the fitted Lorentzian lineshapes.

Fig. 2 shows variation of the vibrational frequencies of T_{2g} (squares), E_g doublet (circles and stars) and A_{1g} (up triangles) modes as a function of pressure. Filled symbols are for increasing pressure runs and open symbols are for decreasing pressure runs. It can be seen that the pressure dependence of the T_{2g} mode is same for both the increasing and the decreasing pressure runs, showing that the pressure hysterisis effects are negligible. The A_{1g} mode was masked by the strong Raman mode of diamond anvils for pressures between 5 and 9 GPa. After 9 GPa, a shoulder appears to the high frequency side of the Raman line from the diamond anvil, which can be the A_{1g} mode. It is likely that the shoulder may arise from the strained part of the diamond anvil. In that case, it will imply that the A_{1g} mode does not appear after 9 GPa. The values of slope $S = d\omega/dP$ in two pressure range 1 GPa $< P <$ 9 GPa and 10 GPa $< P <$ 18 GPa are given in Table 1. Solid lines show the linear least square fit to the data. It is clear from Table 1 and Fig. 2 that the slopes of vibrational frequency ω for T_{2g}, E_g and A_{1g} modes with respect to pressure, change abruptly at about 10 GPa. This pressure is close to the pressure at which the pressure transmitting alcohol medium freezes. Above this, the pressure is quasi-hydrostatic and the nonhydrostatic component in the pressure increases gradually, as reflected in the pressure calibrant ruby luminescence linewidths. The change in slope, $S = d\omega/dP$ at ~10 GPa cannot arise from

Table 1
The values of $d\omega/dP$ and Grüneissen parameters for the different modes region I: 1 GPa ≤ P ≤ 9 GPa and region II: 10 GPa ≤ P ≤ 18 GPa. The value of the bulk modulus, β is taken to be 142 GPa for P ≤ 9 GPa (I) and 125 GPa for P ≥ 10 GPa (II) from the fitted equation of state

Mode	ω at $P = 0$ (cm^{-1})	S (cm^{-1}/GPa)		γ	
		I	II	I	II
T_{2g}	677	3.8	2.0	0.8	0.4
E_g	1116	7.8	–	1.0	–
	1135	6.8	1.0	0.9	0.1
A_{1g}	1251	9.9	0.4	1.1	0.04
T_{1u}	186	−0.8	–	−0.6	–
T_{1g}	438	6.5	–	2.1	–

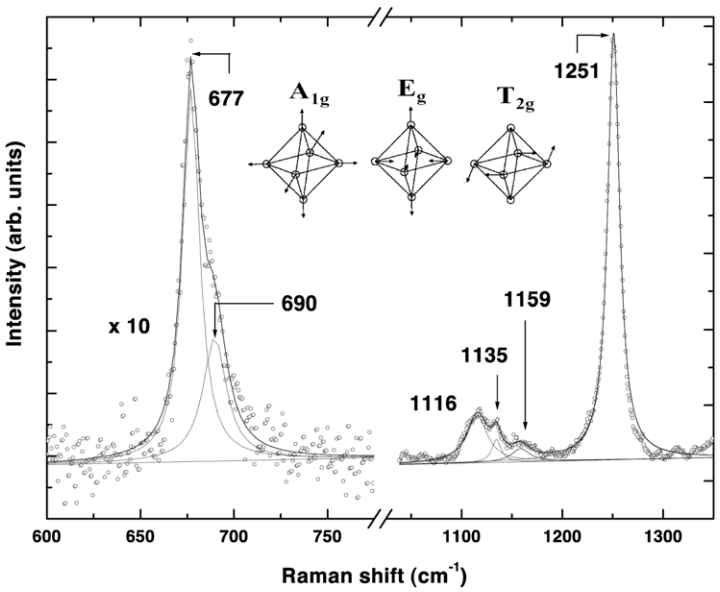

Fig. 1. Raman spectra of LaB_6 at ambient condition.

the gradual change in the nature of applied pressure and hence we attribute the change in slope to a phase transition at 10 GPa in LaB_6. In Fig. 2, we also notice an additional slope change for all the three modes near 1 GPa indicating some possible phase transition. More data is required at low pressures to confirm this transition, if any. The values of S in units of cm^{-1}/GPa and the Grüneissen parameters $\gamma = \beta$ d ln ω/dP, where β is the bulk modulus (taken to be 142 GPa for $P < 10$ GPa and 125 GPa for $P > 10$ GPa as described later) are tabulated in Table 1. The S values for E_g and A_{1g} modes in the range $0 \le P \le 1$ GPa are 18.6, 27.5 and 18.5 cm^{-1}/GPa, respectively and the corresponding Grüneissen parameters are 2.4, 3.5 and 2.1, respectively.

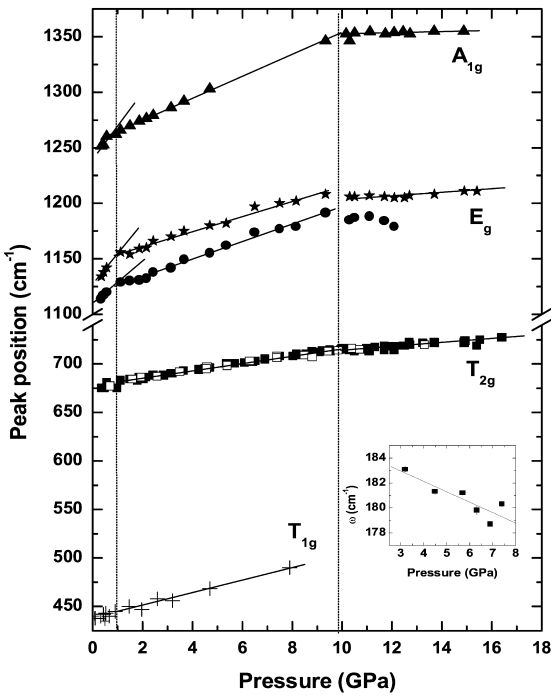

Fig. 2. Variation of A_{1g} mode (triangles), E_g mode (stars and circles), T_{2g} mode (squares) and T_{1g} mode (plus) frequencies with pressure. Solid lines are linear fits. For T_{2g} mode, the filled and open symbols correspond to the increasing and decreasing pressure runs, respectively.

In addition to Raman allowed modes, we also observe modes near 180 and 438 cm^{-1}. The mode near 180 cm^{-1} is easily discernible in spectra recorded at pressures between 3 to 8 GPa. Interestingly, the pressure derivative of this mode is negative, with a slope dω/d$P = -0.8$ cm^{-1}/GPa as shown in the inset of Fig. 2. This mode is the infrared active T_{1u} mode which becomes Raman active, possibly due to disorder in the crystal. This disorder can be interpreted on the basis of the reduced symmetry $O_h \rightarrow C_{4v}$ arising from the presence of vacancies in the B_6 structure [13]. The variation of 438 cm^{-1} mode with pressure is also shown in Fig. 2 where the data is shown by plus signs and is fitted to a straight line, with slope dω/d$P = 6.5$ cm^{-1}/GPa and $\gamma =$ 2.1.

3.2. X-ray diffraction

To confirm the results of Raman experiments, angle dispersive X-ray diffraction (ADXRD) measurements up to 20 GPa were carried out on powdered LaB_6. The measured ambient pressure lattice parameter agreed with the literature value [12] of $a_c = 4.154$ Å. The evolution of the X-ray diffraction pattern under pressure and d-spacing values are shown in Figs. 3 and 4(a), respectively. The X-ray patterns

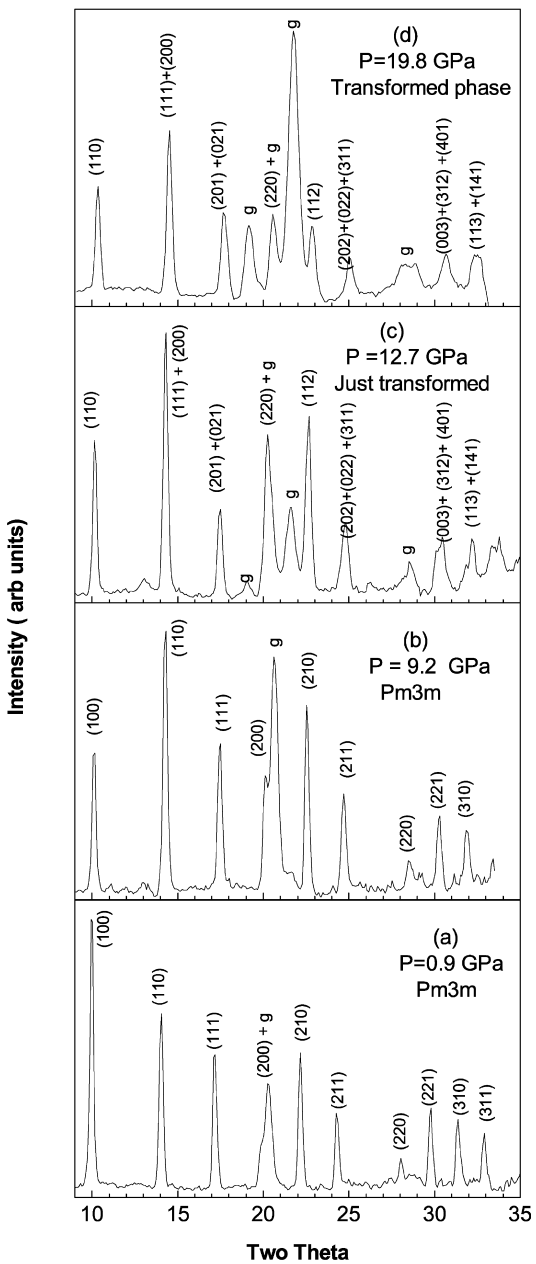

Fig. 3. ADXRD patterns for LaB_6 at various pressures.

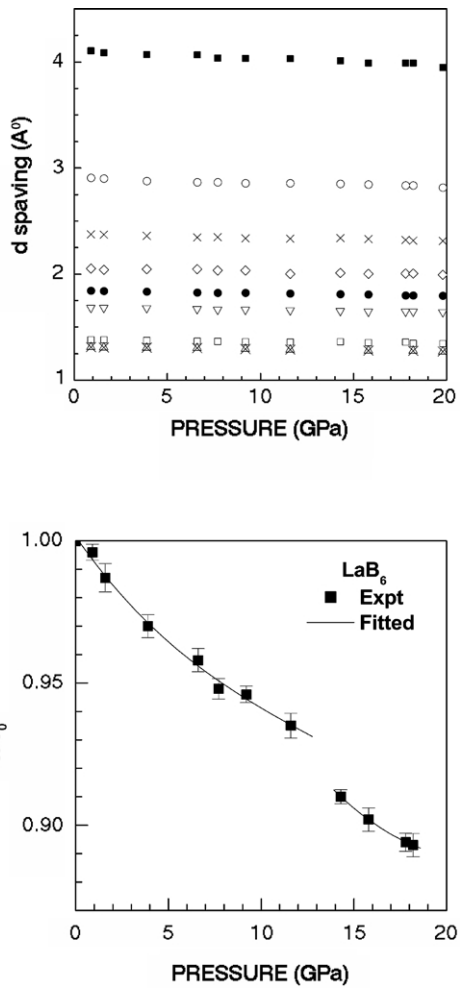

Fig. 4. (a) Variation of d-spacings with pressure for LaB_6. (b) Equation of state for LaB_6. The experimental data points are shown along with the error bars for V/V_0. The solid curves are the fitted curve for the cubic and orthorhombic phases.

could be indexed to the CsCl type cubic cell up to ~11.6 GPa. Above this pressure, the fitting to the cubic phase gradually deteriorates. Our attempt to index the X-ray diffraction pattern above 11.6 GPa to CrB_6 type tetragonal and AsB_6 hexagonal structures did not succeed. The high pressure pattern however could be indexed to an orthorhombic cell with 2 molecular units per cell ($a_0 = 5.619$ Å, $b_0 = 5.732$ Å, $c_0 = 4.051$ Å and $Z = 2$ at 14.3 GPa). This orthorhombic cell is a supercell of the cubic cell ($a_0 \sim \sqrt{2}a_c$, $b_0 \sim \sqrt{2}a_c$ and $c_0 \sim a_c$). The possible space group is Pban with La at the 2a (0,0,0) position and B at the 4l (0,0.5,0.2) and 8m (0.15, 0.36, 0.3359) positions. Further it may be noted that the expected split in the lines because of the lower symmetry is not discernable due to the resolution limitation of the current measurements. Thus although the present data indicate the presence of a subtle transition, better resolution data from well collimated beam from synchrotron is desirable. The pressure–volume data obtained from lattice parameter determination up to 20 GPa is shown in Fig. 4(b). This was fitted to a second order Birch–Murnaghan equation of state [14] with a bulk modulus β of 142 GPa for the cubic phase with its pressure derivative $d\beta/dP = 4$. If the statistical errors in volume are included in the calculation of bulk modulus, we obtain a bulk modulus of 142 ± 15 GPa for the low pressure phase

which compares well with the value of 163 GPa obtained from elastic constant measurements [3]. The effect of structural phase transition on the equation of state is clearly seen as a discontinuity around 11 GPa. This can be seen as a weak slope change in the d variarion with pressure for the first two lines. Thus it is observed that the transition is weakly first order as the volume change at the transition is small (less than 2%).

3.3. Band structure calculations

First principles electronic structure calculations of metallic LaB_6 can throw light on the mechanism of the structural phase transition. Hasegawa and Yanase [15] have carried out self-consistent augmented plane wave calculations of band structure of LaB_6. However, their calculations were carried out using muffin–tin approximation to the atomic spheres and smaller number of k-points in sampling the Brillouin zone (BZ).They also used Slater Xα-method for the exchange potential. In order to improve upon these limitations we have done ab-initio electronic structure calculations using full potential linear augmented plane wave (FPLAPW) method within the local density approximation (LDA) for the exchange correlation [16]. Spin–orbit correction terms were included in the calculations. For all the calculations reported here we have used WIEN2K code as described by Blaha et al. [17]. $5d^16s^2$ electrons of La and $2s^22p^1$ of B were treated as itinerant. 10000 k-points (286 k-points for the irreducible wedge of the BZ) were used for BZ sampling. To represent the wave functions in the interstitial region, 615 plane waves were used. Band structure was calculated at 0.01 interval of volume ratio V/V_0. For each volume the pressure was computed by evaluating the volume derivative of the total energy–volume curve at its minimum. Computations were carried out up to a volume compression of $V/V_0 = 0.85$. In this paper we will give only one result of our calculations, represented in Fig. 5 which shows that at ambient condition, the position of the band minimum (d-band) is 0.8 mRy below E_F shown in bottom panel. These features in band structure are in qualitative agreement with those reported by Hasegawa and Yanase [15]. With compression, this band is up in energy relative to E_F and at $V/V_0 = 0.92$ (i.e. around 13 GPa) it crosses the Fermi level (see middle panel in Fig. 5). At a compression of $V/V_0 = 0.85$, the band minimum is above the Fermi level as seen in Fig. 5. Thus anomalies in some of the physical properties could occur at $V/V_0 = 0.92$ if the same structure was maintained [18]. This kind of phase transition driven by changes in the topology of the Fermi surface is called Electronic Topological Transition (ETT) or Lifshitz transition. The theory of ETT has been discussed in detail in the review article by Blanter et al. [19].

To conclude, the Raman and X-ray measurements show a subtle transition around 10 GPa. First principles electronic band calculations reveal that the transition is accompanied by the interception of Fermi level by electronic band extremum.

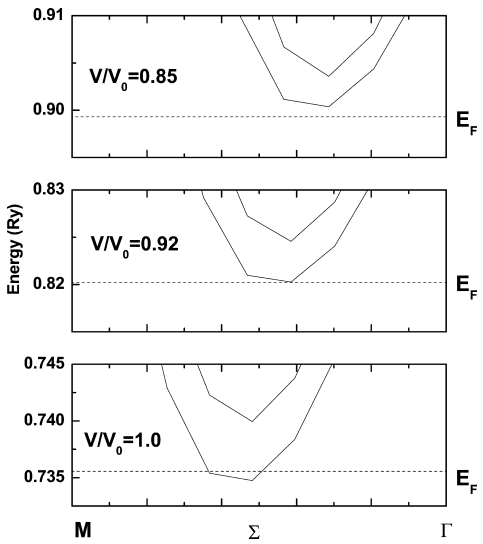

Fig. 5. Position of the band minimum along the Γ–M direction of the Brillouin zone with respect to E_F at different compressions.

Acknowledgements

AKS thanks Dr A. Jayaraman for single crystals of LaB_6, Department of Science and Technology, India for financial support and Dr. C.S. Sunder for initial characterization of the crystals. PVT thanks Council for Scientific and Industrial Research, India for financial assistance.

References

[1] M. Ishii, M. Aono, S. Muranaka, S. Kawai, Solid State Commun. 20 (1976) 437.
[2] M. Nakasuji, H. Wada, J. Vac. Sci. Technol. 17 (1980) 1367.
[3] T. Tanaka, J. Yoshimoto, M. Ishii, E. Bannai, S. Kawai, Solid State Commun. 22 (1977) 203.
[4] T. Kasuya, M. Kasaya, K. Takegahara, T. Fujita, T. Goto, A. Tamaki, M. Takigawa, H. Yasuka, J. Magn. Magn. Mat. 31–34 (1983) 447. T. Goto, A. Tamaki, S. Kunii, T. Nakajima, T. Fujimura, T. Kasuya, T. Komatsubara, S.B. Woods, J. Magn. Magn. Mat. 31–34 (1983) 419.
[5] H.G. Smith, et al., Solid State Commun. 53 (1985) 15.
[6] K. Takegahara, T. Kasuya, Solid State Commun. 53 (1985) 21.
[7] V.A. Sidrov, et al., Sov. Phys. Solid State 32 (1989) 1586.
[8] V.A. Sidrov, et al., Sov. Phys. Solid State 32 (1991) 720.
[9] D.V.S. Muthu, P. Teredesai, A. Jayaraman, N. Chandrabhas, A.K. Sood, Solid State Phys. (India) 41 (1998) 136.
[10] S. Meenakshi, V. Vijayakumar, R.S. Rao, B.K. Godwal, S.K. Sikka, Z. Hossain, R. Nagarajan, L.C. Gupta, R. Vijayaraghavan, Physica B 223-224 (1996) 93.

[11] H. Scholz, W. Bauhofer, K. Ploog, Solid State Commun. 18 (1976) 1539.
[12] Z. Yahia, S. Turrell, G. Turrell, J.P. Mercurio, J. Mol. Struct. 224 (1990) 303.
[13] Z. Yahia, S. Turrell, J.P. Mercurio, G. Turrell, J. Raman Spectrosc. 24 (1993) 207.
[14] F.D. Murnaghan, Proc. Natl Acad. Sci. 30 (1944) 244.
[15] A. Hasegawa, A. Yanase, J. Phys. F: Metal Phys. 7 (1977) 1245.
[16] J.P. Perdew, Y. Wang, Phys. Rev. B 45 (1992) 13244.
[17] P. Blaha, K. Schwarz, G.K.H. Madsen, D. Kvasnicka, J. Luitz, WIEN 2K, An Augmented Plane wave + Local Orbitals Program for Calculating Crystal Properties, Techn. Universitat, Wien, Austria, 2001.
[18] L.M. Lifshitz, Sov. Phys. JETP 11 (1960) 1130. L. Dagens, J. Phy. F 8 (1978) 2093.
[19] Ya.M. Blanter, M.I. Kaganov, A.V. Pantsulaya, A.A. Varlamov, Phys. Rep. 245 (1994) 159.